

RESEARCH ARTICLE | OCTOBER 28 2024

High-coherence quantum acoustics with planar superconducting qubits

W. J. M. Franse ; C. A. Potts ; V. A. S. V. Bittencourt ; A. Metelmann ; G. A. Steele  



Appl. Phys. Lett. 125, 183501 (2024)

<https://doi.org/10.1063/5.0230359>



Articles You May Be Interested In

Coupling high-overtone bulk acoustic wave resonators via superconducting qubits

Appl. Phys. Lett. (September 2023)

Temperature evolution of frequency and anharmonic phonon loss for multi-mode epitaxial HBARs

Appl. Phys. Lett. (September 2020)

Toward 40 GHz excitation of diamond-based HBAR

Appl. Phys. Lett. (February 2021)

High-coherence quantum acoustics with planar superconducting qubits

Cite as: Appl. Phys. Lett. **125**, 183501 (2024); doi: [10.1063/5.0230359](https://doi.org/10.1063/5.0230359)

Submitted: 23 July 2024 · Accepted: 12 October 2024 ·

Published Online: 28 October 2024





View Online



Export Citation



CrossMark

W. J. M. Franse,¹  C. A. Potts,^{1,2,3}  V. A. S. V. Bittencourt,⁴  A. Metelmann,^{4,5}  and G. A. Steele^{1,a)} 

AFFILIATIONS

¹Kavli Institute of NanoScience, Delft University of Technology, PO Box 5046, 2600 GA Delft, The Netherlands

²Niels Bohr Institute, University of Copenhagen, Blegdamsvej 17, 2100 Copenhagen, Denmark

³Center for Hybrid Quantum Networks (Hy-Q), Niels Bohr Institute, University of Copenhagen, Copenhagen, Denmark

⁴ISIS (UMR 7006), Université de Strasbourg, 67000 Strasbourg, France

⁵Institute for Theory of Condensed Matter and Institute for Quantum Materials and Technology, Karlsruhe Institute of Technology, 76131 Karlsruhe, Germany

^{a)}Author to whom correspondence should be addressed: g.a.steele@tudelft.nl

ABSTRACT

Quantum acoustics is an emerging platform for hybrid quantum technologies enabling quantum coherent control of mechanical vibrations. High-overtone bulk acoustic resonators (HBARs) represent an attractive mechanical implementation of quantum acoustics due to their potential for exceptionally high mechanical coherence. Here, we demonstrate an implementation of high-coherence HBAR quantum acoustics integrated with a planar superconducting qubit architecture, demonstrating an acoustically induced-transparency regime of high cooperativity and weak coupling, analogous to the electrically induced transparency in atomic physics. Demonstrating high-coherence quantum acoustics with planar superconducting devices enables interesting applications for acoustic resonators in quantum technologies.

© 2024 Author(s). All article content, except where otherwise noted, is licensed under a Creative Commons Attribution (CC BY) license (<https://creativecommons.org/licenses/by/4.0/>). <https://doi.org/10.1063/5.0230359>

In the field of quantum acoustodynamics (cQAD), superconducting transmon qubits^{1–3} have been coupled to multiple different forms of mechanical modes such as propagating surface acoustic (SAW),^{4–7} film bulk acoustic resonators (FBARs),⁸ ultra-high-frequency (UHF) nanoresonator,⁹ nanomechanical resonators,^{10,11} and high-overtone bulk acoustic resonator (HBAR) coupled to either 3D^{12–14} or 2D transmons.^{15–18} The potential applications of HBAR quantum acoustic devices include compact quantum memories,¹⁹ quantum interfaces to spin devices,^{20,21} microwave to optical quantum transduction,²² and the exploration of fundamental mass limits in quantum mechanics.^{23,24}

An attractive feature of HBARs is the small surface-to-volume ratio of the acoustic modes, enabling them to exploit the exceptionally high bulk mechanical quality factor of crystalline materials, with bulk modes whose quality factor can exceed 10^{10} .²⁵ While the pioneering work¹² with HBARs achieved moderate quality factors of 10^5 , quality factors of 10^6 were soon achieved^{13,26} by shaping the top piezo element to reduce diffraction by shaping the acoustic mode, creating an effective acoustic plano-convex lens.

Initial work in the field focused on superconducting qubits in 3D architecture, which enables high-coherence times of the superconducting qubit.¹² While it can be more difficult to engineer the same

coherence times in planar qubit devices, the planar approach offers significant advantages, such as the ease of integrating multiple qubits on the same chip. The planar design also enables the inclusion of fast-flux lines for rapid control of qubit frequencies and qubit couplings and enables high-speed parametric modulation for applications such as parametric amplifiers and on-chip circulators.²⁷ The integration of acoustic devices with planar superconducting circuits would provide a valuable quantum resource but, until now, attempts to integrate HBARs with planar circuits have resulted in reduced coherence of the mechanical modes^{15,17} exhibiting quality factors on the order of 10^3 – 10^4 .

Here, we demonstrate the integration of HBAR devices with state-of-the-art mechanical coherence with a planar superconducting qubit chip. Our architecture is based on a flip-chip assembly of a piezoelectric HBAR chip on top of a superconducting qubit chip fabricated on a silicon wafer using standard circuit QED processes and designs. We observe sharp HBAR resonances inside a broad qubit linewidth, whose mechanical nature is confirmed by changing the qubit frequency through multiple resonances via AC-Stark tuning with a nearby drive tone. To decouple the effect of the hybridization of the HBAR mode with the qubit, the resulting lineshapes are analyzed using a master equation simulation to extract the intrinsic mechanical

damping rate.²⁸ Doing so, we extract intrinsic damping rates 6.8 kHz, corresponding to Q-factors of 9.0×10^5 , despite the absence of any mechanical lensing engineered in the piezo actuation layer, promising for the integration of HBARs with more complex superconducting circuits for applications in quantum technologies.

The device has two feedlines with five multiplexed readout resonators coupled to five niobium-titanium nitride transmon qubits. The top line has the flipped HBAR chip aligned with the transmon qubits, and the bottom line is an exact copy without the HBAR chip for control measurements. In this flip-chip architecture, the top chip consists of five cylindrical-shaped aluminum nitride piezoelectric transducers on a sapphire substrate. The bottom chip includes superconducting transmons and coplanar waveguide readout resonators on a silicon substrate, see Figs. 1(a) and 1(c). An optical micrograph of a single transmon qubit with an HBAR is shown in Fig. 1(b); the piezoelectric cylinder is visible as a large circle exhibiting white light interference. The interference pattern suggests a gap between the piezoelectric disk and the silicon substrate on the order of $1 \mu\text{m}$.

To excite HBAR modes near 6 GHz most efficiently, the piezoelectric layer was designed to have a thickness of $t_p \approx 900 \text{ nm}$. Since the resonance frequency of the piezoelectric disk is given by $f_0 = v_p/2t_p$, where v_p is the acoustic velocity in the piezoelectric material ($v_{\text{AlN}} \approx 1.14 \times 10^4 \text{ m/s}$). The mode spacing between two consecutive resonances, the free spectral range (FSR), of the phononic resonator is given by $f_{\text{FSR}} = v_s/2t_s$, where v_s is the acoustic velocity in sapphire ($\sim 1.11 \times 10^4 \text{ m/s}$) and t_s is the HBAR thickness, with a predicted FSR of 8.538 MHz for a $650 \mu\text{m}$ sapphire substrate.

The flip-chip device was cooled to a temperature of $\sim 20 \text{ mK}$ in a commercial dilution refrigerator. We measured our readout resonator $\omega_r = 2\pi \times 4.910 \text{ GHz}$ to be 1.07 GHz detuned from our qubit's ground-to-excited state transition frequency $\omega_{\text{eg}} = 2\pi \times 6.067 \text{ GHz}$.

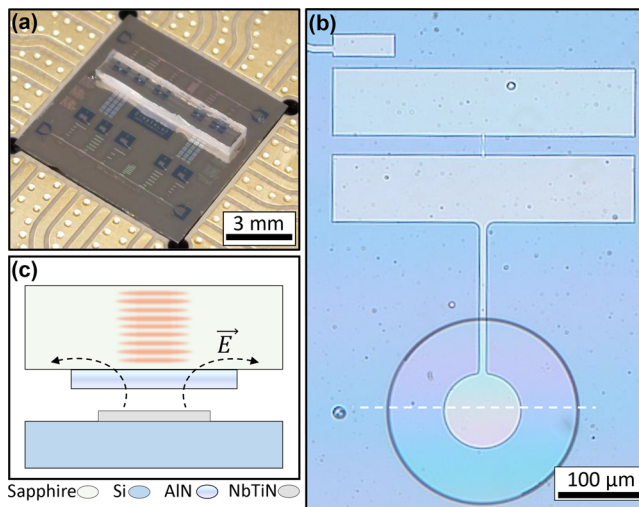


FIG. 1. A planar Transmon flip-chip HBAR device. (a) Photo of the assembled device. (b) Optical image of transmon with HBAR on top. White light interference fringes in HBAR suggest a gap distance of a few micrometers between the top and bottom chip. (c) Schematic side view of assembly drawn at the dashed white line in (b). The antenna of the transmon qubit emits an alternating electric field, \vec{E} , to actuate the piezoelectric, which, in turn, generates a standing wave in the sapphire substrate.

To confirm coupling to HBAR resonances, we use the AC-Stark effect^{29–31} to shift the qubit's resonance frequency. The Stark drive was applied to the qubit detuned 30 MHz above the qubit frequency, $\omega_{\text{Stark}} = 2\pi \times 6.09605 \text{ GHz}$. Increasing the Stark tone's power while performing two-tone spectroscopy shifts the qubit to lower frequencies, see Fig. 2. In this measurement, a high-power qubit probe tone is applied such that power broadening allows the simultaneous measurement of multiple HBAR resonances within the qubit linewidth. The sharp resonances occur every 8.53 MHz, in excellent agreement with the designed FSR.

In order to quantify the interaction strength of the qubit and the phonon modes, additional two-tone spectroscopy was performed with sufficient resonator probe power and qubit drive power so that only one acoustic mode became visible within the qubit peak. To optimize measurement time, we performed segmented qubit drive frequency sweeps: In a span of 200 kHz around the acoustic mode, frequency points were spaced 250 Hz apart, but in a larger span of 20 MHz around the qubit ω_{eg} transition, they were spaced 250 kHz apart. The data (gray dots) are shown in Fig. 3, where panel (a) shows full acoustically induced transparency (AIT) of qubit with one coupled acoustic mode and (b) shows a zoom-in of the HBAR mode.

Figure 3 shows high-resolution traces of the HBAR AIT resonances observed in qubit spectroscopy taken at low qubit drive and readout resonator drive powers to minimize the broadening of the qubit linewidth. Panel (a) shows a wide sweep in this regime, where the full qubit peak is visible. The qubit spectroscopic peak shows a small

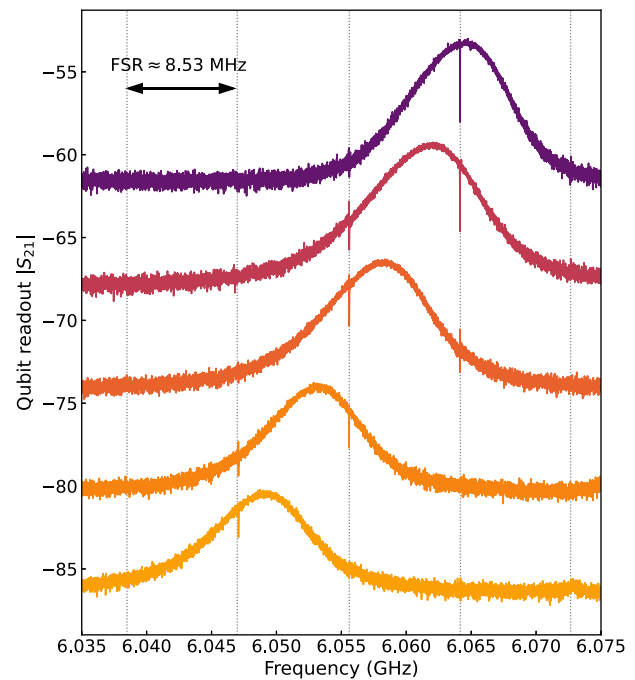


FIG. 2. Observation of multiple HBAR resonances by AC-Stark shifting of the qubit frequency. The qubit $\omega_{\text{eg}}/2\pi$ transition is tuned using a Stark drive tone with small detuning ($\omega_{\text{Stark}}/2\pi = 6.09605 \text{ GHz}$). The curves represent two-tone spectroscopy measurements for different Stark powers (top to bottom: -22.0 , -15.5 , -12.0 , -9.0 , and -7.5 dBm). HBAR resonances are observed at fixed frequencies separated by a free spectral range of 8.53 MHz, corresponding to a $650 \mu\text{m}$ Sapphire substrate.

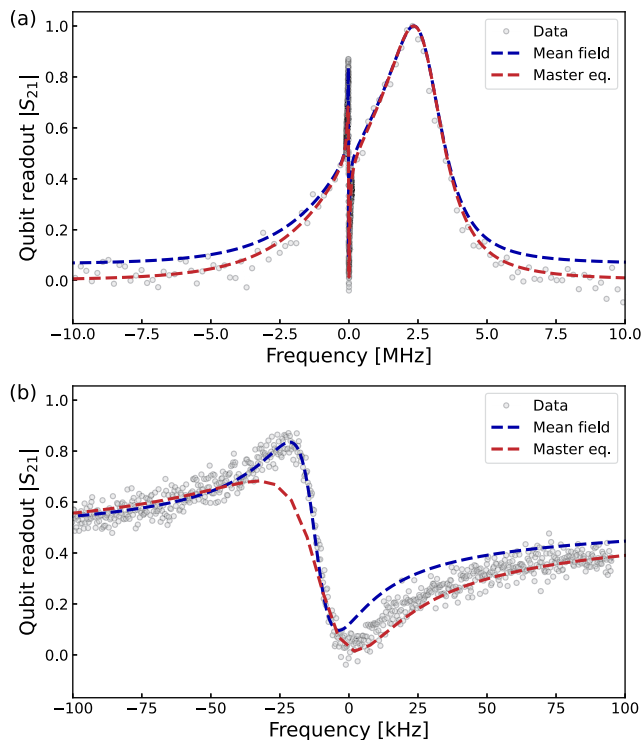


FIG. 3. Extracting the intrinsic mechanical damping rate in the AIT regime. (a) Experimental two-tone data of qubit ground-to-excited state transition coupled to a single HBAR mode at 6.064 GHz (gray dots) at low qubit driving power. Both panels also show the qubit spectrum determined from mean-field (blue dashed line) and master equation simulations (red dashed line). (b) Zoom in on the HBAR resonance. The fit to the mean-field theory determines an intrinsic mechanical damping rate of $\gamma/2\pi = 6.98 \pm 0.03$ kHz, corresponding to a quality factor of 9.0×10^5 and a qubit-phonon coupling $g_{qh}/2\pi = 197 \pm 1$ kHz. In panels (a) and (b), frequency refers to the detuning from the HBAR mode.

degree of asymmetry in its line shape, which we attribute to the residual thermal occupation of the readout resonator, see Ref. 28. The line indicates the result of a master equation and mean-field calculations of the qubit spectroscopy. The mean-field curve was used to extract the intrinsic damping rate of the mechanical mode by fitting the data. We note that even at low powers, the qubit has a relatively large linewidth of 425 kHz. While it is likely that dielectric losses from the piezoelectric can reduce qubit coherence, in our case, the reference qubits on the chip which were not coupled to the HBARs also showed comparable linewidths, suggesting the piezoelectric layer, in this case, is not the source of qubit decay. We currently believe that the large linewidth in our qubit fabrication process is related to an interaction of the aluminum layer of the qubit with a silicon layer that was overetched during the base layer patterning.

Figure 3(b) shows a zoom of the AIT feature with high spectral resolution along with the calculations. From the mean-field model, we extract an intrinsic mechanical damping rate of the HBAR mode of 6.98 ± 0.03 kHz, describing the mechanical decay rate if the HBAR were decoupled from the qubit entirely and a qubit-HBAR coupling rate of 197 ± 1 kHz. We note that the spectroscopic AIT feature observed in the experimental spectroscopy can be not only broader than the intrinsic

mechanical linewidth due to hybridization with the qubit but also narrower than the intrinsic mechanical linewidth at higher qubit drive powers due to mechanical amplification and narrowing stemming from single-atom lasing physics.²⁸ As described in the previous work,²⁸ there is good agreement between the calculation and the experiment. However, we can see here that the master equation simulations performed failed to capture a slight bump on the left side of the AIT feature. This feature can be captured better by mean-field calculations.²⁸ In any case, both mean-field and master equation modeling describe the behavior of the data and can be used to extract similar line widths.

Interestingly, we achieved state-of-the-art mechanical coherence, comparable to the best HBARs in 3D qubit architectures, in the absence of any shaping of the piezo surface to produce acoustic lensing. It is interesting to ask why the etched piezo shaping is not needed on our device. One possibility is that the small qubit electrode combined with the large piezo disk may already provide some electrostatic lensing from the non-uniform electric fields in the piezoelectric material, something which could be explored in future work. The high coherence demonstrated here, in any case, opens up an exciting route to combining quantum acoustics with planar technologies such as fast-flux lines, flux-mediated parametric gates,³² SNAILS,³³ and asymmetrically threaded SQUIDs.³⁴

See the [supplementary material](#) for details on device fabrication, mean-field calculations, and reference qubit data.

W.J.M.F. and G.A.S. acknowledge support through the QUAKE project, project number 680.92.18.04, of the research programme Natuurkunde Vrije Programma's of the Dutch Research Council (NWO). C.A.P. acknowledges the support of the Natural Sciences and Engineering Research Council of Canada (NSERC). A.M. and V.A.S.V.B. acknowledge financial support from the Contrat Triennal 2021-2023 Strasbourg Capitale Européenne.

AUTHOR DECLARATIONS

Conflict of Interest

The authors have no conflicts to disclose.

Author Contributions

W. J. M. Franse: Data curation (lead); Formal analysis (equal); Investigation (lead); Methodology (lead); Software (lead); Visualization (lead); Writing – original draft (equal); Writing – review & editing (equal). **C. A. Potts:** Data curation (equal); Formal analysis (equal); Methodology (equal); Supervision (equal); Writing – original draft (equal); Writing – review & editing (equal). **V. A. S. V. Bittencourt:** Formal analysis (supporting); Software (supporting); Writing – review & editing (supporting). **A. Metelmann:** Funding acquisition (supporting); Project administration (supporting); Supervision (supporting); Validation (supporting). **G. A. Steele:** Conceptualization (equal); Funding acquisition (equal); Project administration (equal); Supervision (equal); Validation (equal); Writing – review & editing (equal).

DATA AVAILABILITY

The data that support the findings of this study are openly available in Zenodo at <https://doi.org/10.5281/zenodo.13881198>, Ref. 35.

REFERENCES

- ¹A. Wallraff, D. I. Schuster, A. Blais, L. Frunzio, J. Majer, M. H. Devoret, S. M. Girvin, and R. J. Schoelkopf, "Approaching unit visibility for control of a superconducting qubit with dispersive readout," *Phys. Rev. Lett.* **95**, 060501 (2005).
- ²D. I. Schuster, A. A. Houck, J. A. Schreier, A. Wallraff, J. M. Gambetta, A. Blais, L. Frunzio, J. Majer, B. Johnson, M. H. Devoret, S. M. Girvin, and R. J. Schoelkopf, "Resolving photon number states in a superconducting circuit," *Nature* **445**, 515–518 (2007).
- ³J. Koch, T. M. Yu, J. Gambetta, A. A. Houck, D. I. Schuster, J. Majer, A. Blais, M. H. Devoret, S. M. Girvin, and R. J. Schoelkopf, "Charge-insensitive qubit design derived from the cooper pair box," *Phys. Rev. A* **76**, 042319 (2007).
- ⁴M. V. Gustafsson, T. Aref, A. F. Kockum, M. K. Ekström, G. Johansson, and P. Delsing, "Propagating phonons coupled to an artificial atom," *Science* **346**, 207–211 (2014).
- ⁵K. J. Satzinger, Y. P. Zhong, H.-S. Chang, G. A. Peairs, A. Bienfait, M.-H. Chou, A. Y. Cleland, C. R. Conner, É. Dumur, J. Grebel, I. Gutierrez, B. H. November, R. G. Povey, S. J. Whiteley, D. D. Awschalom, D. I. Schuster, and A. N. Cleland, "Quantum control of surface acoustic-wave phonons," *Nature* **563**, 661–665 (2018).
- ⁶A. Bienfait, K. J. Satzinger, Y. P. Zhong, H.-S. Chang, M.-H. Chou, C. R. Conner, É. Dumur, J. Grebel, G. A. Peairs, R. G. Povey, and A. N. Cleland, "Phonon-mediated quantum state transfer and remote qubit entanglement," *Science* **364**, 368–371 (2019).
- ⁷C. Undershute, J. M. Kitzman, C. A. Mikolas, and J. Pollanen, "Decoherence of surface phonons in a quantum acoustic system," [arXiv:2410.03005](https://arxiv.org/abs/2410.03005) (2024).
- ⁸A. O'Connell, M. Hofheinz, M. Ansmann, R. Bialczak, M. Lenander, E. Lucero, M. Neeley, D. Sank, H. Wang, M. Weides, J. Wenner, J. Martinis, and A. Cleland, "Quantum ground state and single-phonon control of a mechanical resonator," *Nature* **464**, 697–703 (2010).
- ⁹F. Rouxinol, Y. Hao, F. Brito, A. O. Caldeira, E. K. Irish, and M. D. LaHaye, "Measurements of nanoresonator-qubit interactions in a hybrid quantum electromechanical system," *Nanotechnology* **27**, 364003 (2016).
- ¹⁰P. Arrangoiz-Arriola and A. H. Safavi-Naeini, "Engineering interactions between superconducting qubits and phononic nanostructures," *Phys. Rev. A* **94**, 063864 (2016).
- ¹¹P. Arrangoiz-Arriola, E. A. Wollack, Z. Wang, M. Pechal, W. Jiang, T. P. McKenna, J. D. Witmer, R. V. Laer, and A. H. Safavi-Naeini, "Resolving the energy levels of a nanomechanical oscillator," *Nature* **571**, 537–540 (2019).
- ¹²Y. Chu, P. Kharel, W. H. Renninger, L. D. Burkhardt, L. Frunzio, P. T. Rakich, and R. J. Schoelkopf, "Quantum acoustics with superconducting qubits," *Science* **358**, 199–202 (2017).
- ¹³Y. Chu, P. Kharel, T. Yoon, L. Frunzio, P. T. Rakich, and R. J. Schoelkopf, "Creation and control of multi-phonon Fock states in a bulk acoustic-wave resonator," *Nature* **563**, 666–670 (2018).
- ¹⁴V. Jain, V. D. Kurilovich, Y. D. Dahmani, C. U. Lei, D. Mason, T. Yoon, P. T. Rakich, L. I. Glazman, and R. J. Schoelkopf, "Acoustic radiation from a superconducting qubit: From spontaneous emission to Rabi oscillations," *Phys. Rev. Appl.* **20**, 014018 (2023).
- ¹⁵M. Kervinen, I. Rissanen, and M. Sillanpää, "Interfacing planar superconducting qubits with high overtone bulk acoustic phonons," *Phys. Rev. B* **97**, 205443 (2018).
- ¹⁶M. Kervinen, J. E. Ramí rez-Muñoz, A. Välimaa, and M. A. Sillanpää, "Landau-Zener-Stückelberg interference in a multimode electromechanical system in the quantum regime," *Phys. Rev. Lett.* **123**, 240401 (2019).
- ¹⁷M. Kervinen, A. Välimaa, J. E. Ramí rez-Muñoz, and M. A. Sillanpää, "Sideband control of a multimode quantum bulk acoustic system," *Phys. Rev. Appl.* **14**, 054023 (2020).
- ¹⁸A. Välimaa, W. Crump, M. Kervinen, and M. A. Sillanpää, "Multiphonon transitions in a quantum electromechanical system," *Phys. Rev. Appl.* **17**, 064003 (2022).
- ¹⁹C. T. Hann, C.-L. Zou, Y. Zhang, Y. Chu, R. J. Schoelkopf, S. M. Girvin, and L. Jiang, "Hardware-efficient quantum random access memory with hybrid quantum acoustic systems," *Phys. Rev. Lett.* **123**, 250501 (2019).
- ²⁰E. MacQuarrie, T. Gosavi, N. Jungwirth, S. Bhawe, and G. Fuchs, "Mechanical spin control of nitrogen-vacancy centers in diamond," *Phys. Rev. Lett.* **111**, 227602 (2013).
- ²¹H. Chen, N. F. Opondo, B. Jiang, E. R. MacQuarrie, R. S. Daveau, S. A. Bhawe, and G. D. Fuchs, "Engineering electron-phonon coupling of quantum defects to a semiconfocal acoustic resonator," *Nano Lett.* **19**, 7021–7027 (2019).
- ²²T. Blésin, H. Tian, S. A. Bhawe, and T. J. Kippenberg, "Quantum coherent microwave-optical transduction using high-overtone bulk acoustic resonances," *Phys. Rev. A* **104**, 052601 (2021).
- ²³M. F. Gely and G. A. Steele, "Superconducting electro-mechanics to test Diósi-Penrose effects of general relativity in massive superpositions," *AVS Quantum Sci.* **3**, 035601 (2021).
- ²⁴M. Bild, M. Fadel, Y. Yang, U. von Lüpke, P. Martin, A. Bruno, and Y. Chu, "Schrödinger cat states of a 16-microgram mechanical oscillator," *Science* **380**, 274–278 (2023).
- ²⁵S. Galliou, M. Goryachev, R. Bourquin, P. Abbé, J. P. Aubry, and M. E. Tobar, "Extremely low loss phonon-trapping cryogenic acoustic cavities for future physical experiments," *Sci. Rep.* **3**, 2132 (2013).
- ²⁶U. von Lüpke, Y. Yang, M. Bild, L. Michaud, M. Fadel, and Y. Chu, "Parity measurement in the strong dispersive regime of circuit quantum acoustodynamics," *Nat. Phys.* **18**, 794–799 (2022).
- ²⁷R. Navarathna, D. T. Le, A. R. Hamann, H. D. Nguyen, T. M. Stace, and A. Fedorov, "Passive superconducting circulator on a chip," *Phys. Rev. Lett.* **130**, 037001 (2023).
- ²⁸C. Potts, W. Franse, V. Bittencourt, A. Metelmann, and G. Steele, "A superconducting single-atom phonon laser," [arXiv:2312.13948](https://arxiv.org/abs/2312.13948) (2023).
- ²⁹M. Brune, P. Nussenzweig, F. Schmidt-Kaler, F. Bernardot, A. Maali, J. M. Raimond, and S. Haroche, "From lamb shift to light shifts: Vacuum and sub-photon cavity fields measured by atomic phase sensitive detection," *Phys. Rev. Lett.* **72**, 3339–3342 (1994).
- ³⁰D. I. Schuster, A. Wallraff, A. Blais, L. Frunzio, R.-S. Huang, J. Majer, S. M. Girvin, and R. J. Schoelkopf, "ac stark shift and dephasing of a superconducting qubit strongly coupled to a cavity field," *Phys. Rev. Lett.* **94**, 123602 (2005).
- ³¹J. Gambetta, A. Blais, D. I. Schuster, A. Wallraff, L. Frunzio, J. Majer, M. H. Devoret, S. M. Girvin, and R. J. Schoelkopf, "Qubit-photon interactions in a cavity: Measurement-induced dephasing and number splitting," *Phys. Rev. A* **74**, 042318 (2006).
- ³²N. Didier, E. A. Sete, J. Combes, and M. P. da Silva, "Ac flux sweet spots in parametrically modulated superconducting qubits," *Phys. Rev. Appl.* **12**, 054015 (2019).
- ³³V. Sivak, N. Frattini, V. Joshi, A. Lingenfelter, S. Shankar, and M. Devoret, "Kerr-free three-wave mixing in superconducting quantum circuits," *Phys. Rev. Appl.* **11**, 054060 (2019).
- ³⁴R. Lescanne, M. Villiers, T. Peronnin, A. Sarlette, M. Delbecq, B. Huard, T. Kontos, M. Mirrahimi, and Z. Leghtas, "Exponential suppression of bit-flips in a qubit encoded in an oscillator," *Nat. Phys.* **16**, 509–513 (2020).
- ³⁵C. Potts (2024). "Figure for: High-coherence quantum acoustics with planar superconducting qubits," Zenodo. <https://doi.org/10.5281/zenodo.13881198>